Prompt photon hadroproduction at high energies in the k_T-factorization approach

A.V. Lipatov, N.P. Zotov

July 20, 2005

D.V. Skobeltsyn Institute of Nuclear Physics,
M.V. Lomonosov Moscow State University,
*119992 Moscow, Russia*

Abstract

We consider the prompt photon production at high energy hadron colliders in the framework of k_T-factorization approach. The unintegrated quark and gluon distributions in a proton are determined using the Kimber-Martin-Ryskin prescription. The conservative error analisys is performed. We investigate both inclusive prompt photon and prompt photon and associated muon production rates. In Standard Model such events come mainly due to Compton scattering process where the final heavy (charm or bottom) quark produces a muon. The theoretical results are compared with recent experimental data taken by the D⊘ and CDF collaborations at Fermilab Tevatron. Our analysis also covers the azimuthal correlations between produced prompt photon and muon which can provide an important information about non-collinear parton evolution in a proton. Finally, we extrapolate the theoretical predictions to CERN LHC energies.

1   Introduction

It is well known that production of prompt (or direct) photons at high energies has provided a direct probe of the hard subprocess dynamics, since produced photons are largely insensitive to the final-state hadronization effects. Hadroproduction of prompt photons has been studied in a number of experiments [1–5]. Usually photons are called "prompt" if they are coupled to the interacting quarks. In the framework of Quantum Chromodynamics (QCD) the dominant production mechanism for the prompt photons at Tevatron and LHC colliders is the Compton scattering $gq \to \gamma q$ [6]. It is clear that cross section of such processes is sensitive to the gluon distributions in a proton. Also observed final state photon

arXiv:hep-ph/0507243 v1   20 Jul 2005
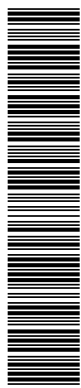
may arise from so called fragmentation processes [7], where a quark or gluon is transformed into γ. The cross sections of such processes involve relative poorly known parton-to-photon fragmentation functions [8]. However, the isolation criterion which is usually introduced in experimental analyses substantially reduces the fragmentation component (see, for example, Ref. [9]). Therefore for the theoretical description of prompt photon production at Tevatron the detailed knowledge of parton (quark and gluon) distributions in a proton is necessary.

Usually quark and gluon densities in a proton are described by the Dokshitzer-Gribov-Lipatov-Altarelli-Parizi (DGLAP) evolution equation [10] where large logarithmic terms proportional to $\ln \mu^2$ are taken into account only. The cross sections can be rewritten in terms of process-dependent hard matrix elements convoluted with universal quark and/or gluon density functions. In this way the dominant contributions come from diagrams where parton emissions in initial state are strongly ordered in virtuality. This is called collinear factorization, as the strong ordering means that the virtuality of the parton entering the hard scattering matrix elements can be neglected compared to the large scale μ.

However, at high energies (or small $x \sim \mu^2/s \ll 1$) effects of finite virtualities and transverse momenta of the incoming partons may become more and more important. These effects can be systematically accounted for in the k_T-factorization QCD approach [10–14]. Just as for DGLAP, in this way it is possible to factorize an observable into a convolution of process-dependent hard matrix elements with universal parton distributions. But as the virtualities (and transverse momenta) of the emitted partons are no longer ordered, the matrix elements have to be taken off-shell and the convolution made also over transverse momentum $\mathbf{k}_T$ with the unintegrated (i.e. k_T-dependent) parton distributions. The unintegrated parton distribution $f_a(x, \mathbf{k}_T^2)$ determines the probability to find a type a parton carrying the longitudinal momentum fraction x and the transverse momentum $\mathbf{k}_T$. In particular, usage of the unintegrated parton densities have the advantage that it takes into account true kinematics of the process under consideration even at leading order.

The unintegrated parton distributions $f_a(x, \mathbf{k}_T^2)$ are a subject of intensive studies [15, 16]. Various approaches to investigate these quantities has been proposed. It is believed that at assymptotically large energies (or very small x) the theoretically correct description is given by the Balitsky-Fadin-Kuraev-Lipatov (BFKL) evolution equation [17] where large terms proportional to $\ln 1/x$ are taken into account. Another approach, valid for both small and large x, have been developed by Ciafaloni, Catani, Fiorani and Marchesini, and is known as the CCFM model [18]. It introduces angular ordering of emissions to correctly treat gluon coherence effects. In the limit of asymptotic energies, it almost equivalent to the BFKL [19–21], but also similar to the DGLAP evolution for large $x \sim 1$. The resulting unintegrated gluon distribution depends on two scales, the additional scale $\bar{q}$ is a variable related to the maximum angle allowed in the emission and plays the role of the evolution scale μ in the collinear parton densities.

The two-scale involved unintegrated parton distributions it is possible to obtain also from the conventional ones using the Kimber-Martin-Ryskin (KMR) prescription [22]. In this way the μ dependence in the unintegrated parton distribution enters only in last step of the evolution, and single scale evolution equations can be used up to this step. Such procedure can be applied to a proton as well as photon and is expected to account for the main part of the conventional next-to-leading logarithmic QCD corrections. The KMR-constructed parton densities were used, in particular, to describe the heavy quark production in $\gamma\gamma$

collisions at CERN LEP2 [23], prompt photon photoproduction at DESY HERA [24] (both inclusive and associated with hadronic jet) and inclusive prompt photon hadroproduction at Fermilab Tevatron [25].

Recently new experimental data on the $p + \bar{p} \to \gamma + X$ process at Tevatron were obtained by the D$\oslash$ [1, 2] and CDF [3, 4] collaborations. It was found [1–4] that the shape of the measured cross sections as a function of photon transverse energy E_T^γ is poorly described by next-to-leading order (NLO) QCD calculations: the observed E_T^γ distribution is steeper than the predictions of perturbative QCD. These shape differences lead to a significant disagreement in the ratio of cross sections calculated at different center-of-mass energies $\sqrt{s} = 630$ GeV and $\sqrt{s} = 1800$ GeV as a function of scaling variable $x_T = 2E_T^\gamma/\sqrt{s}$. The disagreement in the x_T ratio is difficult to explain with conventional theoretical uncertainties connected with scale dependence and parametrizations of the parton distributions [2, 3]. However, such discrepancy can be reduced [26, 27] by introducing some additional intrinsic transverse momentum k_T of the incoming partons, which is usually assumed to have a Gaussian-like distribution [26]. The average value of this k_T increases from $\langle k_T \rangle \sim 0.5$ GeV to more than $\langle k_T \rangle \sim 2$ GeV as the $\sqrt{s}$ increases from UA6 to Tevatron energies [27]. However, in this case the full kinematics of the subprocess is not taken into account, as it was argued in Ref. [25].

The inclusive prompt photon hadroproduction at Tevatron in the k_T-factorization QCD approach was considered in Ref. [25]. The unintegrated parton distributions in a proton were obtained using the KMR formalism. The role of the both non-perturbative and perturbative components of partonic transverse momentum k_T in describing of the observed E_T^γ spectrum was investigated. However, the KMR unintegrated parton densities were obtained in the double leading logarithmic approximation (DLLA) only. Also in these calculations the usual on-shell matrix elements of hard partonic subprocesses were evaluated with precise off-shell kinematics.

In the present paper we apply the KMR method to obtain the unintegrated quark and gluon distributions in a proton $f_a(x, \mathbf{k}_T^2, \mu^2)$ independently from other authors. Then, we study inclusive prompt photon hadroproduction at Tevatron in more detail. We calculate the double differential cross sections $d\sigma/dE_T^\gamma d\eta^\gamma$ at two different center-of-mass energies $\sqrt{s} = 630$ GeV and $\sqrt{s} = 1800$ GeV and compare our theoretical results with the recent D$\oslash$ and CDF experimental data [1–4]. In order to estimate the theoretical uncertainties of our predictions we study the renormalization and factorization scale dependences of calculated cross sections. Also we study the ratio of cross sections calculated at different center-of-mass energies $\sqrt{s} = 630$ GeV and $\sqrt{s} = 1800$ GeV. After that we extrapolate our predictions to LHC energies. In all these calculations we use the expressions for the partonic off-shell matrix elements which were obtained in our previous paper [24].

Also we investigate here the prompt photon and associated muon production at Fermilab Tevatron. In the Standard Model (SM) these events come mainly due to Compton scattering process $g + Q \to \gamma + Q$, where final state muon originates from the semileptonic decay of heavy (charm or bottom) quark Q [5]. It is important that studying of such processes possible can provide an information about new physics beyond the SM [28]. Therefore it is necessary to have a realistic estimation of associated $\gamma + \mu$ production cross sections within the QCD. Such calculations in the k_T-factorization QCD approach are performed for the first time. In order to investigate the underlying dynamics in more detail, we study the azimuthal

3

correlations between the transverse momenta of produced prompt photon and muon. These quantities are sensitive to the different production mechanisms and also are powerful tests for the non-collinear evolution [29, 30].

The our paper is organized as follows. In Section 2 the KMR unintegrated parton densities in a proton are obtained and their properties are discussed. In particular, we compare the KMR gluon distributions with ones obtained from the full CCFM equation and within the framework of the Linked Dipole Chain model [31] (which is reformulation and generalization of the CCFM model). In Section 3 we present the basic formulas with a brief review of calculation steps. In Section 4 we present the numerical results of our calculations. Finally, in Section 5, we give some conclusions.

2 The KMR unintegrated partons

The Kimber-Martin-Ryskin approach [22] is the formalism to construct parton distributions $f_a(x, \mathbf{k}_T^2, \mu^2)$ unintegrated over the parton transverse momenta $\mathbf{k}_T^2$ from the known conventional parton distributions $a(x, \mu^2)$, where $a = xg$ or $a = xq$. This formalism is valid for a proton as well as photon and can embody both DGLAP and BFKL contributions. It also accounts for the angular ordering which comes from coherence effects in gluon emission. The key observation here is that the μ dependence of the unintegrated parton distributions $f_a(x, \mathbf{k}_T^2, \mu^2)$ enters at the last step of the evolution, and therefore single scale evolution equations (DGLAP or unified DGLAP-BFKL [32]) can be used up to this step. Also it was shown [22] that the unintegrated distributions obtained via unified DGLAP-BFKL evolution are rather similar to those based on the pure DGLAP equations. It is because the imposition of the angular ordering constraint is more important than including the BFKL effects. Based on this point, in our calculations we use much more simpler DGLAP equation up to the last evolution step. In this approximation, the unintegrated quark and gluon distributions are given [22] by

$$f_q(x, \mathbf{k}_T^2, \mu^2) = T_q(\mathbf{k}_T^2, \mu^2) \frac{\alpha_s(\mathbf{k}_T^2)}{2\pi} \times$$

$$\times \int\limits_x^1 dz \left[P_{qq}(z) \frac{x}{z} q\left(\frac{x}{z}, \mathbf{k}_T^2\right) \Theta\left(\Delta - z\right) + P_{qg}(z) \frac{x}{z} g\left(\frac{x}{z}, \mathbf{k}_T^2\right) \right], \tag{1}$$

$$f_g(x, \mathbf{k}_T^2, \mu^2) = T_g(\mathbf{k}_T^2, \mu^2) \frac{\alpha_s(\mathbf{k}_T^2)}{2\pi} \times$$

$$\times \int\limits_x^1 dz \left[\sum_q P_{gq}(z) \frac{x}{z} q\left(\frac{x}{z}, \mathbf{k}_T^2\right) + P_{gg}(z) \frac{x}{z} g\left(\frac{x}{z}, \mathbf{k}_T^2\right) \Theta\left(\Delta - z\right) \right], \tag{2}$$

where $P_{ab}(z)$ are the usual unregulated leading order DGLAP splitting functions, and $q(x, \mu^2)$ and $g(x, \mu^2)$ are the conventional quark and gluon densities. The theta functions which appear in (1) and (2) imply the angular-ordering constraint $\Delta = \mu/(\mu + |\mathbf{k}_T|)$ specifically to the last evolution step to regulate the soft gluon singularities. For other evolution steps, the strong ordering in transverse momentum within the DGLAP equations automatically ensures angular ordering. It is important that parton distributions $f_a(x, \mathbf{k}_T^2, \mu^2)$ extended

now into the $\mathbf{k}_T^2 > \mu^2$ region. This fact is in the clear contrast with the usual DGLAP evolution[1].

The virtual (loop) contributions may be resummed to all orders by the quark and gluon Sudakov form factors

$$\ln T_q(\mathbf{k}_T^2, \mu^2) = -\int_{\mathbf{k}_T^2}^{\mu^2} \frac{d\mathbf{p}_T^2}{\mathbf{p}_T^2} \frac{\alpha_s(\mathbf{p}_T^2)}{2\pi} \int_0^{z_{\max}} dz\, P_{qq}(z),$$ (3)

$$\ln T_g(\mathbf{k}_T^2, \mu^2) = -\int_{\mathbf{k}_T^2}^{\mu^2} \frac{d\mathbf{p}_T^2}{\mathbf{p}_T^2} \frac{\alpha_s(\mathbf{p}_T^2)}{2\pi} \left[n_f \int_0^1 dz\, P_{qg}(z) + \int_{z_{\min}}^{z_{\max}} dz\, z\, P_{gg}(z) \right],$$ (4)

where $z_{\max} = 1 - z_{\min} = \mu/(\mu + |\mathbf{p}_T|)$. The form factors $T_a(\mathbf{k}_T^2, \mu^2)$ give the probability of evolving from a scale $\mathbf{k}_T^2$ to a scale μ^2 without parton emission. In according with (3) and (4) $T_a(\mathbf{k}_T^2, \mu^2) = 1$ in the $\mathbf{k}_T^2 > \mu^2$ region.

Note that such definition of the $f_a(x, \mathbf{k}_T^2, \mu^2)$ is correct for $\mathbf{k}_T^2 > \mu_0^2$ only, where $\mu_0 \sim 1$ GeV is the minimum scale for which DGLAP evolution of the collinear parton densities is valid. Everywhere in our numerical calculations we set the starting scale μ_0 to be equal $\mu_0 = 1$ GeV. Since the starting point of this derivation is the leading order DGLAP equations, the unintegrated parton distributions must satisfy the normalisation condition

$$a(x, \mu^2) = \int_0^{\mu^2} f_a(x, \mathbf{k}_T^2, \mu^2) d\mathbf{k}_T^2.$$ (5)

This relation will be exactly satisfied if we define [22]

$$f_a(x, \mathbf{k}_T^2, \mu^2)\big|_{\mathbf{k}_T^2 < \mu_0^2} = a(x, \mu_0^2) T_a(\mu_0^2, \mu^2).$$ (6)

Then, we have obtained the unintegrated parton distributions in a proton. In Figure 1 we show these densities $f_a(x, \mathbf{k}_T^2, \mu^2)$ at scale $\mu^2 = 100\,\text{GeV}^2$ as a function of x for different values of $\mathbf{k}_T^2$, namely $\mathbf{k}_T^2 = 2\,\text{GeV}^2$ (a), $\mathbf{k}_T^2 = 5\,\text{GeV}^2$ (b), $\mathbf{k}_T^2 = 10\,\text{GeV}^2$ (c) and $\mathbf{k}_T^2 = 20\,\text{GeV}^2$ (d). The solid, dashed, short dashed, dotted, dash-dotted and short dash-dotted lines correspond to the unintegrated gluon (divided by factor 10), $u + \bar{u}$, $d + \bar{d}$, s, c and b quark distributions, respectively. We have used here the standard leading-order Glück-Reya-Vogt (GRV) parametrizations [33] of the collinear quark and gluon densities $a(x, \mu^2)$. Note that unintegrated c and b quark distributions at $\mathbf{k}_T^2 = 2\,\text{GeV}^2$ are very similar and cannot be really resolved in Figure 1. Also we have checked numerically that normalization condition (5) is correctly satisfied for all unintegrated parton distributions $f_a(x, \mathbf{k}_T^2, \mu^2)$.

It is interesting to compare the KMR-constructed unintegrated parton densities with the distributions obtained in other approaches. Recently the full CCFM equation in a proton was solved numerically using a Monte Carlo method, and new fits of the unintegrated gluon distributions (J2003 set 1 — 3) have been presented [34]. The input parameters were fitted

---

[1]We would like to note that cut-off Δ can be taken $\Delta = |\mathbf{k}_T|/\mu$ also [25]. In this case the unintegrated parton distributions given by (1) — (2) vanish for $\mathbf{k}_T^2 > \mu^2$ in accordance with the DGLAP strong ordering in $\mathbf{k}_T^2$.

5

to describe the proton structure function $F_2(x, Q^2)$. These unintegrated gluon densities were used also in analysis of the forward jet production at HERA, charm and bottom production at Tevatron [34], and charm and J/ψ production at LEP2 energies [35]. Also three different versions of the unintegrated gluon distributions obtained in the framework of the Linked Dipole Chain (LDC) model have been presented [36]. These gluon densities has been fitted to the inclusive F_2 data at HERA and already were used, in particular, in analysis [37] of the charm and beauty hadroproduction at Tevatron. In Figure 2 we plot the KMR (as a solid lines), the J2003 set 1 (as a dashed lines) unintegrated gluon distributions and so called *standard* version of the LDC unintegrated gluon distribution (as a dash-dotted lines) at scale $\mu^2 = 100 \, \text{GeV}^2$ as a function of x for different values of gluon $\mathbf{k}_T^2$, namely $\mathbf{k}_T^2 = 2 \, \text{GeV}^2$ (a), $\mathbf{k}_T^2 = 10 \, \text{GeV}^2$ (b), $\mathbf{k}_T^2 = 20 \, \text{GeV}^2$ (c) and $\mathbf{k}_T^2 = 50 \, \text{GeV}^2$ (d). One can see that behaviour of different unintegrated parton distributions in the small $\mathbf{k}_T^2$ region (which essentially drives the total cross sections) is very different. At the same time the differences between these distributions tends to be small when gluon transverse momentum $\mathbf{k}_T^2$ is large. Therefore the dependence of our predictions on the evolution scheme possible may be rather large, and further theoretical attempts are necessary to reduce this uncertainty.

3   Calculation details

3.1   The subprocesses under consideration

The main contribution to the prompt photon production in proton-antiproton collisions at Tevatron and LHC colliders comes from quark-gluon and quark-antiquark induced partonic subprocesses:

$$q(k_1) + g(k_2) \to \gamma(p^\gamma) + q(p'), \tag{7}$$

$$q(k_1) + \bar{q}(k_2) \to \gamma(p^\gamma) + g(p'), \tag{8}$$

where the particles four-momenta are given in parentheses. Additionally, photons can be produced through the fragmentation of a partonic jet into a single photon carrying a large fraction z of the jet energy [7]. These processes are described in terms of quark-to-photon $D_{q \to \gamma}(z, \mu^2)$ and gluon-to-photon $D_{g \to \gamma}(z, \mu^2)$ fragmentation functions [8]. The main feature of the fragmentation contribution in leading order is fact that produced jet is balanced by a photon on the opposite side of the event and accompanied by collinear photon on the same side of the event.

It is important that in order to reduce the huge background from the secondary photons produced by the decays of π^0 and η mesons the isolation criterion is introduced in the experimental analyses. This criterion is the following. A photon is isolated if the amount of hadronic transverse energy E_T^{had}, deposited inside a cone with aperture R centered around the photon direction in the pseudo-rapidity and azimuthal angle plane, is smaller than some value E_T^{max}:

$$\begin{aligned} E_T^{\text{had}} &\leq E_T^{\text{max}}, \\ (\eta - \eta^\gamma)^2 + (\phi - \phi^\gamma)^2 &\leq R^2. \end{aligned} \tag{9}$$

The both D⊘ and CDF collaborations take $R \sim 0.4$ and $E_T^{\text{max}} \sim 1$ GeV in the experiment [1–5]. Isolation not only reduces the background but also significantly reduces the fragmentation

components. It was shown [38] that after applying the isolation cut (9) the contribution from the fragmentation subprocesses is about 10% of the total cross section. Since the dependence of our results on the non-collinear parton evolution scheme may be rather large (as it was demonstrated in Section 2), in our further analysis we will neglect the relative small fragmentation contribution and consider only the $q + g \to \gamma + q$ and $q + \bar{q} \to \gamma + g$ subprocesses. We would like to note that photon produced in these processes is isolated from the quark or gluon jet by requiring a non-zero transverse momentum of a photon or jet in the $p\bar{p}$ center-of-mass frame.

3.2 Kinematics

Let p_1 and p_2 be the four-momenta of the incoming protons. The initial off-shell partons have the four-momenta k_1 and k_2. In our analysis below we will use the Sudakov decomposition, which has the following form:

$$p^\gamma = \alpha_1 p_1 + \beta_1 p_2 + p_T^\gamma, \quad p' = \alpha_2 p_1 + \beta_2 p_2 + p_T', $$
$$k_1 = x_1 p_1 + k_{1T}, \quad k_2 = x_2 p_2 + k_{2T}, \tag{7}$$

where k_{1T}, k_{2T}, p_T^γ and p_T' are the transverse four-momenta of the corresponding particles. It is important that $\mathbf{k}_{1T}^2 = -k_{1T}^2 \neq 0$ and $\mathbf{k}_{2T}^2 = -k_{2T}^2 \neq 0$. In the $p\bar{p}$ center-of-mass frame we can write

$$p_1 = \sqrt{s}/2(1, 0, 0, 1), \quad p_2 = \sqrt{s}/2(1, 0, 0, -1), \tag{8}$$

where $s = (p_1 + p_2)^2$ is the total energy of the process under consideration and we neglect the masses of the incoming protons. The Sudakov variables are expressed as follows:

$$\alpha_1 = \frac{E_T^\gamma}{\sqrt{s}} \exp(y^\gamma), \quad \alpha_2 = \frac{m_T'}{\sqrt{s}} \exp(y'),$$
$$\beta_1 = \frac{E_T^\gamma}{\sqrt{s}} \exp(-y^\gamma), \quad \beta_2 = \frac{m_T'}{\sqrt{s}} \exp(-y'), \tag{9}$$

where E_T^γ and m_T' are the transverse enegy and transverse mass of produced photon and outgoing parton, respectively, and y^γ and y' are their rapidities (in the $p\bar{p}$ center-of-mass frame). The photon pseudo-rapidity η^γ is defined as $\eta^\gamma = -\ln\tan(\theta^\gamma/2)$, where θ^γ is the polar angle of the prompt photon with respect to the proton beam. From the conservation laws we can easily obtain the following conditions:

$$x_1 = \alpha_1 + \alpha_2, \quad x_2 = \beta_1 + \beta_2, \quad \mathbf{k}_{1T} + \mathbf{k}_{2T} = \mathbf{p}_T^\gamma + \mathbf{p}_T'. \tag{10}$$

The scaling variable $x_T = 2E_T^\gamma/\sqrt{s}$ is also often used in analysis of the prompt photon production.

3.3 Cross section for prompt photon production

The total cross section for prompt photon hadroproduction at high energies in the k_T-factorization QCD approach can be written as

$$d\sigma(p + \bar{p} \to \gamma + X) = \sum_{a,b} \int \frac{dx_1}{x_1} f_a(x_1, \mathbf{k}_{1T}^2, \mu^2) d\mathbf{k}_{1T}^2 \frac{d\phi_1}{2\pi} \times$$
$$\times \int \frac{dx_2}{x_2} f_b(x_2, \mathbf{k}_{2T}^2, \mu^2) d\mathbf{k}_{2T}^2 \frac{d\phi_2}{2\pi} d\hat{\sigma}(ab \to \gamma c), \tag{11}$$

where $a \ldots c = q$ and/or g, $\hat{\sigma}(ab \to \gamma c)$ is the cross section of the photon production in the corresponding parton-parton interaction. Here initial partons a and b have longitudinal momentum fractions x_1 and x_2, non-zero transverse momenta $\mathbf{k}_{1T}$ and $\mathbf{k}_{2T}$ and azimuthal angles ϕ_1 and ϕ_2. From the expression (11) we can easily obtain the formula:

$$
\sigma(p + \bar{p} \to \gamma + X) = \sum_{a,b} \int \frac{E_T^\gamma}{8\pi(x_1 x_2 s)^2} |\bar{\mathcal{M}}|^2(ab \to \gamma c) \times
$$
$$
\times f_a(x_1, \mathbf{k}_{1T}^2, \mu^2) f_b(x_2, \mathbf{k}_{2T}^2, \mu^2) d\mathbf{k}_{1T}^2 d\mathbf{k}_{2T}^2 dE_T^\gamma dy^\gamma dy^c \frac{d\phi_1}{2\pi} \frac{d\phi_2}{2\pi} \frac{d\phi^\gamma}{2\pi},
$$

(12)

where $|\bar{\mathcal{M}}|^2(ab \to \gamma c)$ is the hard partonic squared off-mass shell matrix element which depends on the transverse momenta $\mathbf{k}_{1T}^2$ and $\mathbf{k}_{2T}^2$, y^c is the rapidity of the parton c in the $p\bar{p}$ center-of-mass frame, ϕ_1, ϕ_2 and ϕ^γ are the azimuthal angles of the initial partons a, b and produced prompt photon, respectively. The analytic expression for the $|\bar{\mathcal{M}}|^2(ab \to \gamma c)$ was obtained in our previous paper [24]. We would like to note that if we average the expression (12) over $\mathbf{k}_{1T}$ and $\mathbf{k}_{2T}$ and take the limit $\mathbf{k}_{1T}^2 \to 0$ and $\mathbf{k}_{2T}^2 \to 0$, then we obtain well-known expression for the prompt photon hadroproduction in leading-order (LO) perturbative QCD.

The multidimensional integration in (12) has been performed by means of the Monte Carlo technique, using the routine VEGAS [39]. The full C++ code is available from the authors on request[2].

4 Numerical results

We now are in a position to present our numerical results. First we describe our theoretical input and the kinematical conditions. After we fixed the unintegrated parton distributions in a proton $f_a(x, \mathbf{k}_T^2, \mu^2)$, the cross section (12) depends on the energy scale μ. As it often done [38] for prompt photon production, we choose the factorization and renormalization scales to be equal $\mu_F = \mu_R = \mu = \xi E_T^\gamma$. In order to estimate the theoretical uncertainties of our calculations we will vary the scale parameter ξ between $1/2$ and 2 about the default value $\xi = 1$. Also we use LO formula for the strong coupling constant $\alpha_s(\mu^2)$ with $n_f = 3$ active (massless) quark flavours and $\Lambda_{\mathrm{QCD}} = 232$ MeV, such that $\alpha_s(M_Z^2) = 0.1169$. In our analysis we not neglect the charm and bottom quark masses and set them to be $m_c = 1.5$ GeV and $m_b = 4.75$ GeV, respectively.

4.1 Inclusive prompt photon production at Tevatron

Experimental data [1–4] for the inclusive prompt photon hadroproduction $p + \bar{p} \to \gamma + X$ come from both the D∅ and CDF collaborations. The D∅ [1, 2] data were obtained in the central and forward pseudo-rapidity regions for two different center-of-mass energies, namely $\sqrt{s} = 630$ GeV and $\sqrt{s} = 1800$ GeV. The central pseudo-rapidity region is defined by the requirement $|\eta^\gamma| < 0.9$, and the forward one is defined by $1.6 < |\eta^\gamma| < 2.5$. The more recent CDF data [3] refer to the same central kinematical region $|\eta^\gamma| < 0.9$ for both beam energies $\sqrt{s} = 630$ GeV and $\sqrt{s} = 1800$ GeV. Also very recently the CDF collaboration has

---

[2]lipatov@theory.sinp.msu.ru

presented a new measurement [4] of the prompt photon cross section at $\sqrt{s} = 1800$ GeV. This measurement is based on events where the photon converts into an electron-positron pair in the material of inner detector, resulting in a two track event signature ("conversion" data). These data refer only to the central kinematical region. Actually, there are two different datasets, which were used in the CDF measurement with conversions, namely 8 GeV electron data and 23 GeV photon data[3]. In all these measurements the double differential cross sections $d\sigma/dE_T^\gamma d\eta^\gamma$ as a function of the transverse energy E_T^γ are determined.

The results of our calculations are shown in Figs. 3 — 9. So, Figs. 3 and 4 confront the cross sections $d\sigma/dE_T^\gamma d\eta^\gamma$ calculated at $\sqrt{s} = 630$ GeV in different kinematical regions with the D⊘ [2] and CDF [3] data. The solid lines are obtained by fixing both the factorization and renormalization scales at the default value $\mu = E_T^\gamma$ whereas upper and lower dashed lines correspond to the $\mu = E_T^\gamma/2$ and $\mu = 2E_T^\gamma$ scales, respectively. One can see that our predictions agree with the experimental data within the scale uncertainties. However, the results of calculation with the default scale tend to underestimate the data in the central kinematical region and agree with the D⊘ data in the forward η^γ region. The collinear NLO QCD calculations [38] give the similar description of the data: the results of measurement are higher than the NLO prediction at low E_T^γ in the central η^γ range but agree at all E_T^γ in the forward pseudo-rapidity region. Then, one can see that the scale dependence of our results is rather large: the variation in μ as it was described above changes the cross sections by about 20 — 30%. The theoretical uncertainties of the collinear NLO calculations are similar (about 20%) [2]. However, one should keep in mind that additional dependence of our results on the evolution scheme may be also rather large (as it was discussed in Section 2), and overall agreement with the experimental data can be improved when unintegrated quark and gluon distributions in a proton will be studied more detail. At the same time the use of different sets of the parton distributions in NLO calculations changes the cross sections by less than 5% [2, 3].

The double differential cross sections $d\sigma/dE_T^\gamma d\eta^\gamma$ compared with the experimental data at $\sqrt{s} = 1800$ GeV in different pseudo-rapidity regions are shown in Figs. 5 — 7. All curves here are the same as in Fig. 3. We find that our predictions agree well with the D⊘ [1] and CDF [3, 4] data both in normalization and shape. There are only rather small overestimation of the data at low E_T^γ values in Figs. 6 and 7. Again, the scale dependence of our calculations is about 20 — 30%. The theoretical uncertainties of the collinear NLO predictions are much smaller, about 6% [1]. Note that now NLO calculations agree with the data more qualitatively. So, the shape of the measured cross sections is generally steeper than that of the NLO predictions. It was shown [3, 4] that this shape difference is difficult to explain simply by changing the renormalization/factorization scales in the collinear calculation, or the set of parton distribution functions.

Also the disagreement between data and NLO calculations is visible [2, 3] in the ratio of the cross sections at different energies. This quantity is known as a very informative subject of investigations and provides a precise test of the QCD calculations. It is because many factors which affect the absolute normalization, as well as many theoretical and experimental uncertainties partially or completely cancel out [2, 3]. In particular, the cross section ratio provides a direct probe of the matrix elements of the hard partonic subprocesses since the

---

[3]See Ref. [4] for more details.

theoretical uncertainties due to the quark and gluon distributions are reduced.

So, the D⊘ collaboration has published the results of measurement [2] for the ratio of 630 GeV and 1800 GeV dimensionless cross sections σ_D as a function of scaling variable x_T. The measured cross section σ_D averaged over azimuth is defined as

$$\sigma_D = \frac{1}{2\pi}(E_T^\gamma)^3 \frac{d\sigma}{dE_T^\gamma d\eta^\gamma}. \tag{13}$$

The ratio $\sigma_D(630\,\text{GeV})/\sigma_D(1800\,\text{GeV})$ compared with the D⊘ experimental data [2] in different pseudo-rapidity η^γ regions is shown in Figs. 8 and 9. The solid lines represent the k_T-factorization predictions at default scale μ. For comparison we show also the results of the collinear leading-order (LO) QCD calculations with the GRV parton densities [33] of a proton (as a dashed lines). Note that when we perform the LO QCD calculations we take into account the partonic subprocesses (7) and (8) and neglect the small fragmentation contributions, as it was done in the k_T-factorization case. It is clear that although the experimental points have large errors they tend to support the k_T-factorization predictions. We would like to point out again that now sensitivity of our results to the non-collinear evolution scheme is minimized. In the collinear approach, the NLO corrections improve the description of the data and then sum of LO and NLO contributions practically coincides with our results at $x_T > 0.05$ [2]. This fact is clear indicates that the main part of the collinear high-order corrections is already included at leading-order level in the k_T-factorization formalism[4]. Nevertheless, the experimental data at the lowest x_T are systematically higher [2] than NLO QCD predictions in both central and forward pseudo-rapidity regions, and it was claimed [3] that ratio of the two cross sections as a function of the x_T is difficult to reconcile with the NLO QCD calculations.

4.2   Associated prompt photon and muon production at Tevatron

Now we investigate the prompt photon and associated muon production at Tevatron. These events are assumed to come from associated prompt photon and heavy (charm or bottom) quark production with the heavy quark decaying into a muon [5]. To calculate muon production from heavy quarks we first convert charm (bottom) quarks into D (B) hadrons using the Peterson fragmentation function [40] and then simulate their semileptonic decay according to Standard Model. Our default set of the fragmentation parameters and branching rations is $\epsilon_c = 0.06$, $f(c \to \mu) = 10.2\%$ and $\epsilon_b = 0.06$, $f(b \to \mu) = 10.8\%$. Of course, muon transverse momenta spectra are sensitive to the fragmentation functions. However, this dependence is expected to be small as compared with the scale uncertainties and the uncertainties connected with unintegrated parton densities. On the other hand, the variations of ϵ_c and ϵ_b do not affect on the azimuthal angle distribution (which is one of the main subject of our study) because a fragmentation does not change the direction of the quark or hadron momentum.

The experimental data for the $\gamma + \mu$ cross section at Tevatron come from CDF collaboration [5]. The differential cross section $d\sigma/dp_T^\gamma$ at $\sqrt{s} = 1800$ GeV was obtained. The photon pseudo-rapidity is required to be within $|\eta^\gamma| < 0.9$ region whereas the muon transverse momentum and pseudo-rapidity are required to be $p_T^\mu > 4$ GeV and $|\eta^\mu| < 1.0$.

---

[4]See Refs. [15, 16] for more details.

The transverse momentum distribution $d\sigma/dp_T^\gamma$ in comparison to experimental data [5] is shown in Fig. 10. All curves here are the same as in Fig. 3. One can see that the shape of this distribution is well described by our calculations. However, the theoretical results slightly overestimate the data in absolute normalization. This fact can be connected with the GRV [33] parametrization of charm and bottom collinear densities of a proton (which are one of the basic ingredients of our derivation). Note, however, that in general the experimental points still lie within scale uncertainties (about 30%) of our calculations. It is important also that our predictions practically coincide with the results of collinear NLO QCD calculations [41], which are much larger than LO ones [5]. This fact clearly demonstrates again that the main part of the standard high-order corrections is already effectively included in the k_T-factorization approach.

Further understanding of the process dynamics and in particular of the high-order effects may be obtained from the angular correlation between the transverse momenta of the final state particles. It was shown [30] that investigation of these correlations is a powerful test for the non-collinear parton evolution dynamics. This is because such quantities are sensitive to relative contributions of different production mechanisms to the total cross section. So, in the collinear LO approximation, the prompt photon and heavy quark Q are produced back-to-back. Therefore distribution over the azimuthal angle difference $\Delta\phi^{\gamma Q}$ must be simply a delta function at $\Delta\phi^{\gamma Q} = \pi$. Taking into account the non-vanishing initial parton transverse momenta $\mathbf{k}_{1T}$ and $\mathbf{k}_{2T}$ leads to the violation of this back-to-back kinematics in the k_T-factorization approach.

The differential cross section $d\sigma/d\Delta\phi^{\gamma\mu}$ calculated at $p_T^\mu > 4$ GeV, $|\eta^\mu| < 1.0$ and $|\eta^\gamma| < 0.9$ is shown in Fig. 11. The solid and both dashed lines here are the same as in Fig. 3. The LO QCD contribution also shown (as a dash-dotted line). One can see a clear difference in shape between k_T-factorization results and collinear LO QCD ones. As it was expected, the LO QCD predicts only a peak at $\Delta\phi^{\gamma\mu} = \pi$. The small broadering of $\Delta\phi^{\gamma\mu}$ distribution illustrates the effect of $Q \to \mu$ decays. Unfortunately, the predictions of the NLO QCD for this distribution are still unknown. The direct comparison between NLO calculations and our results should give a number of interesting insighs. In particular, it can provide an important information about high-order terms which are missed in the leading-order k_T-factorization approach. In any case, the future theoretical and experimental study of such processes will be important check of non-collinear parton evolution.

4.3   Inclusive prompt photon production at LHC

We can conclude from Figs. 3 — 11 that our calculations in general agree well with experimental data [1–5] taken by the D⊘ and CDF collaborations at Tevatron. Based on this point, now we can try to extrapolate our theoretical predictions to LHC energies. We perform the calculation for both central and forward pseudo-rapidities η^γ. As a representative example, we will define the central and forward kinematical regions by the requirements $|\eta^\gamma| < 2.5$ and $2.5 < |\eta^\gamma| < 4$, respectively.

The transverse energy E_T^γ distributions of the inclusive prompt photon production in different η^γ ranges at $\sqrt{s} = 14$ TeV are shown in Figs. 12 and 13. All curves here are the same as in Fig. 3. One can see that variation in scale μ changes the estimated cross sections by about 20 — 30%. However, as it was already discussed above, there are additional theoretical

uncertainties due to the non-collinear parton evolution, and these uncertainties are not well studied up to this time. Also the extrapolation of the available parton distribution to the region of lower x is a special problem at the LHC energies. In particular, one of the problem is connected with the correct treatment of saturation effects in small x region[5]. Therefore much more work needs to be done until these uncertainties will be reduced.

5   Conclusions

We present calculations of the prompt photon hadroproduction at high energies in the k_T-factorization QCD approach. In order to obtain the unintegrated quark and gluon distributions in a proton we have used the Kimber-Martin-Ryskin prescription. We have investigated both inclusive prompt photon and associated with muon production rates. The associated $\gamma + \mu$ events come primarily due to the Compton scattering process $g + Q \to \gamma + Q$, with the final state heavy (charm or bottom) quark Q producing a muon. The calculations of such cross sections in the k_T-factorization approach were performed for the first time.

We have found that our predictions for the inclusive prompt photon production agree well with experimental data taken by the D$\oslash$ and CDF collaborations at Tevatron in both central and forward pseudo-rapidity regions. It is very important that perfect agreement was found also in the ratio of two cross sections calculated at $\sqrt{s} = 630$ GeV and $\sqrt{s} = 1800$ GeV. This ratio provides a direct probe of the QCD matrix elements since in this case the theoretical uncertainties connected to the parton distributions are significantly reduced. We have also demonstrated that the main part of the standard high-order corrections is already included in the k_T-factorization formalism at LO level. Additionally, we present our predictions for the inclusive prompt photon production at LHC.

At the same time our results for associated $\gamma + \mu$ production tend to overestimate the CDF data but still agree with data within the scale uncertainties. We have demonstrated also the significant deviation from back-to-back kinematics in prompt photon and associated muon production. We can expect that further theoretical and experimental study of such processes will give an important information about non-collinear parton evolution dynamics.

In order to investigate the theoretical uncertainties of our results we have studied the sensitivity of our predictions to the renormalization and factorization scales. We have found that this dependence is about 20 — 30% in wide center-of-mass energy range. There are, of course, also additional uncertainties due to unintegrated parton distributions in a proton. Therefore much more work needs to be done before these uncertainties will be reduced. Finally, in our analysis we neglect the contribution from the fragmentation processes. We plan to investigate these problems in more detail in the forthcoming publications.

6   Acknowledgements

---

[5]See also Ref. [16] for more information

References

[1] B. Abbott *et al.* (D∅ Collaboration), Phys. Rev. Lett. **84**, 2786 (2000).

[2] V.M. Abazov *et al.* (D∅ Collaboration), Phys. Rev. Lett. **87**, 251805 (2001).

[3] D. Acosta *et al.* (CDF Collaboration), Phys. Rev. **D65**, 112003 (2002).

[4] D. Acosta *et al.* (CDF Collaboration), Phys. Rev. **D70**, 032001 (2004).

[5] T. Affolder *et al.* (CDF Collaboration), Phys. Rev. **D65**, 012003 (2002).

[6] W. Vogelsang and A. Vogt, Nucl. Phys. **B453**, 334 (1995).

[7] K. Koller, T.F. Walsh and P.M. Zerwas, Z. Phys. **C2**, 197 (1979).

[8] A. Gehrmann-De Ridder, G. Kramer and H. Spiesberger, Eur. Phys. J. **C11**, 137 (1999).

[9] M. Fontannaz, J.Ph. Guillet and G. Heinrich, Eur. Phys. J. **C21**, 303 (2001).

[10] V.N. Gribov and L.N. Lipatov, Yad. Fiz. **15**, 781 (1972);
L.N. Lipatov, Sov. J. Nucl. Phys. **20**, 94 (1975);
G. Altarelly and G. Parizi, Nucl. Phys. **B126**, 298 (1977);
Y.L. Dokshitzer, Sov. Phys. JETP **46**, 641 (1977).

[11] V.N. Gribov, E.M. Levin and M.G. Ryskin, Phys. Rep. **100**, 1 (1983).

[12] E.M. Levin, M.G. Ryskin, Yu.M. Shabelsky and A.G. Shuvaev, Sov. J. Nucl. Phys. **53**, 657 (1991).

[13] S. Catani, M. Ciafoloni and F. Hautmann, Nucl. Phys. **B366**, 135 (1991).

[14] J.C. Collins and R.K. Ellis, Nucl. Phys. **B360**, 3 (1991).

[15] B. Andersson *et al.* (Small-x Collaboration), Eur. Phys. J. **C25**, 77 (2002).

[16] J. Andersen *et al.* (Small-x Collaboration), Eur. Phys. J. **C35**, 67 (2004).

[17] E.A. Kuraev, L.N. Lipatov and V.S. Fadin, Sov. Phys. JETP **44**, 443 (1976);
E.A. Kuraev, L.N. Lipatov and V.S. Fadin, Sov. Phys. JETP **45**, 199 (1977);
I.I. Balitsky and L.N. Lipatov, Sov. J. Nucl. Phys. **28**, 822 (1978).

[18] M. Ciafaloni, Nucl. Phys. **B296**, 49 (1988);
S. Catani, F. Fiorani, and G. Marchesini, Phys. Lett. **B234**, 339 (1990);
S. Catani, F. Fiorani, and G. Marchesini, Nucl. Phys. **B336**, 18 (1990);
G. Marchesini, Nucl. Phys. **B445**, 49 (1995).

[19] J.R. Forshaw and A. Sabio Vera, Phys. Lett. **B440**, 141 (1998).

[20] B.R. Webber, Phys. Lett. **B444**, 81 (1998).

[21] G.P. Salam, JHEP **03**, 009 (1999).

[22] M.A. Kimber, A.D. Martin and M.G. Ryskin, Phys. Rev. **D63**, 114027 (2001).

[23] L. Motyka and N. Timneanu, Eur. Phys. J. **C27**, 73 (2003).

[24] A.V. Lipatov and N.P. Zotov, hep-ph/0506044.

[25] M.A. Kimber, A.D. Martin and M.G. Ryskin, Eur. Phys. J. **C12**, 655 (2000).

[26] H.-L. Lai and H.-N. Li, Phys. Rev. **D58**, 114020 (1998).

[27] L. Apanasevich *et al.*, Phys. Rev. **D59**, 074007 (1999).

[28] T. Affolder *et al.* (CDF Collaboration), Phys. Rev. **D65**, 052006 (2002).

[29] M.G. Ryskin, Yu.M. Shabelski and A.G. Shuvaev, Phys. Atom. Nucl. **64**, 1995 (2001).

[30] S.P. Baranov, N.P. Zotov and A.V. Lipatov, Phys. Atom. Nucl. **67**, 824 (2004).

[31] B. Andersson, G. Gustafson and J. Samuelson, Nucl. Phys. **B467**, 443 (1996);
B. Andersson, G. Gustafson and H. Kharraziha, Phys. Rev. **D57**, 5543 (1998).

[32] J. Kwiecinski, A.D. Martin and A.M. Stasto, Phys. Rev. **D56**, 3991 (1997).

[33] M. Glück, E. Reya and A. Vogt, Phys. Rev. **D46**, 1973 (1992);
M. Glück, E. Reya and A. Vogt, Z. Phys. **C67**, 433 (1995).

[34] H. Jung, Mod. Phys. Lett. **A19**, 1 (2004).

[35] A.V. Lipatov and N.P. Zotov, Eur. Phys. J. **C41**, 163 (2005).

[36] G. Gustafson, L. Lönnblad and G. Miu, JHEP **09**, 005 (2002).

[37] A.V. Lipatov, L. Lönnblad and N.P. Zotov, JHEP **01**, 010 (2004).

[38] H. Baer, J. Ohnemus and J.F. Owens, Phys. Rev. **D42**, 1280 (1990).

[39] G.P. Lepage, J. Comput. Phys. **27**, 192 (1978).

[40] C. Peterson, D. Schlatter, I. Schmitt and P. Zervas, Phys. Rev. **D27**, 105 (1983).

[41] B. Bailey, E.L. Berger and L.E. Gordon, Phys. Rev. **D54**, 1896 (1996).
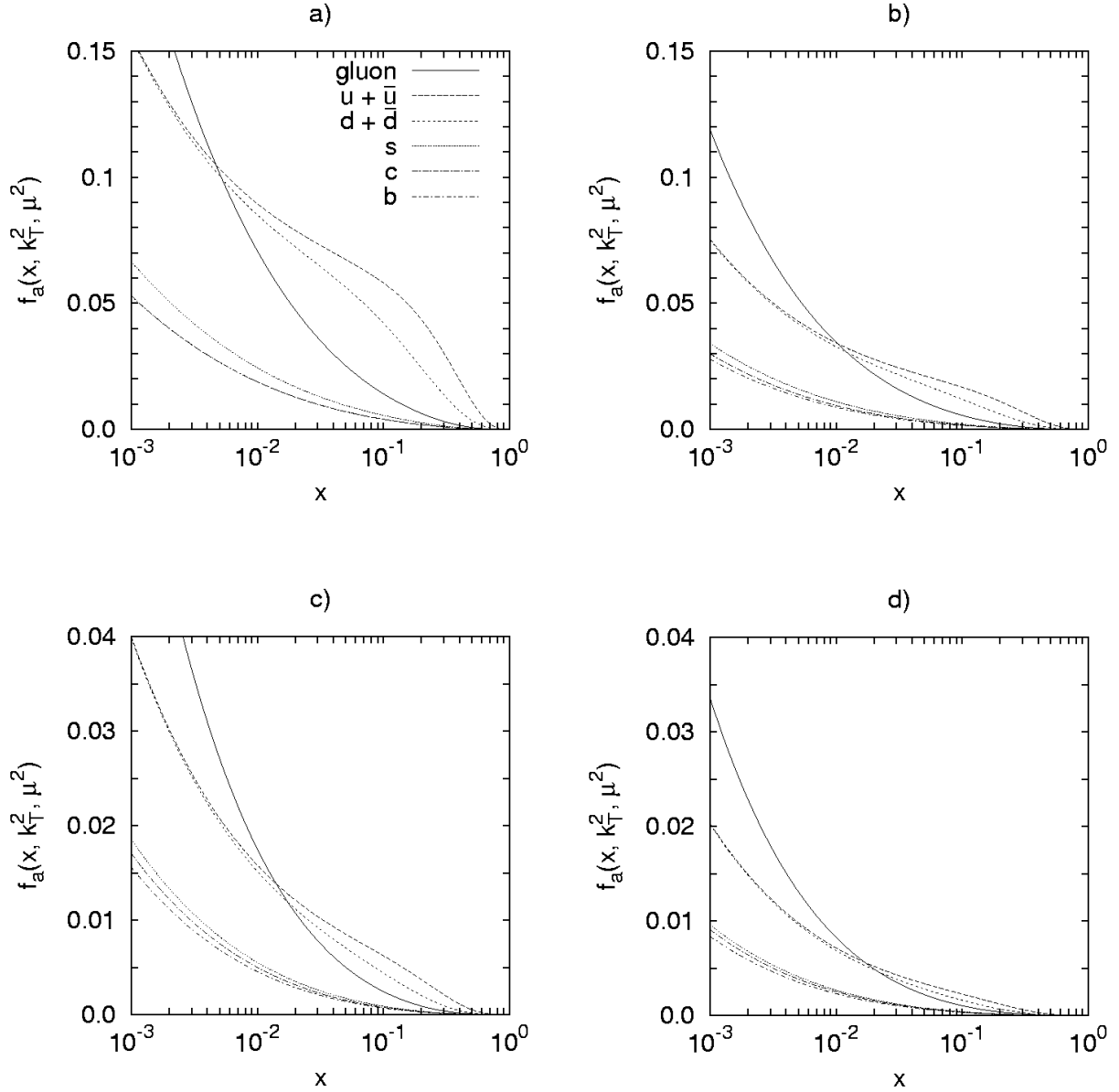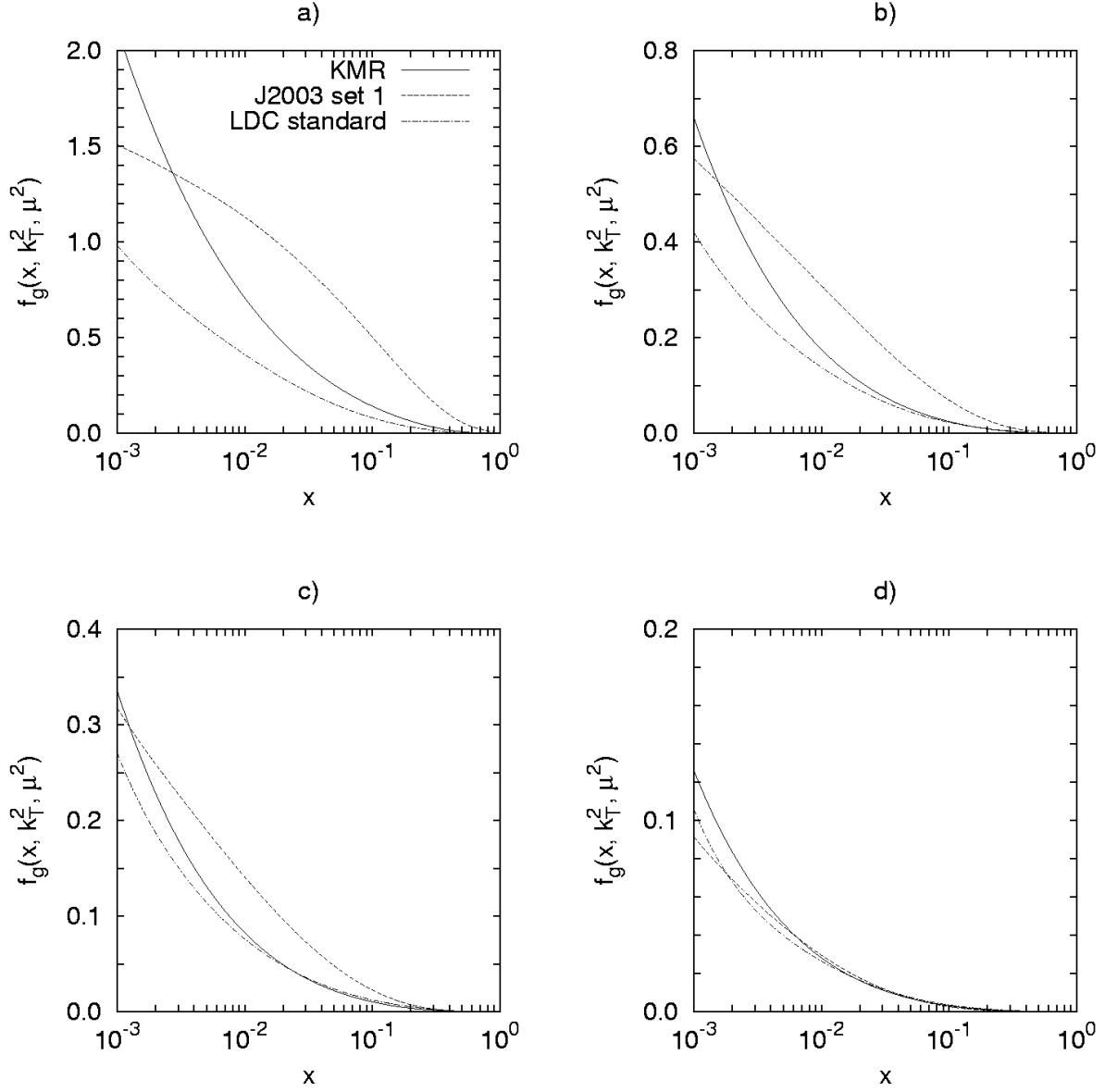
Figure 1: The unintegrated parton distributions $f_a(x, \mathbf{k}_T^2, \mu^2)$ at scale $\mu^2 = 100\,\mathrm{GeV}^2$ as a function of x for different values of $\mathbf{k}_T^2$, namely $\mathbf{k}_T^2 = 2\,\mathrm{GeV}^2$ (a), $\mathbf{k}_T^2 = 5\,\mathrm{GeV}^2$ (b), $\mathbf{k}_T^2 = 10\,\mathrm{GeV}^2$ (c) and $\mathbf{k}_T^2 = 20\,\mathrm{GeV}^2$ (d). The solid, dashed, short dashed, dotted, dash-dotted and short dash-dotted lines correspond to the unintegrated gluon (divided by factor 10), $u + \bar{u}$, $d + \bar{d}$, s, c and b quark distributions, respectively.

15

Figure 2: The unitegrated gluon distributions $f_g(x, \mathbf{k}_T^2, \mu^2)$ at scale $\mu^2 = 100\,\mathrm{GeV}^2$ as a function of x for different values of $\mathbf{k}_T^2$, namely $\mathbf{k}_T^2 = 2\,\mathrm{GeV}^2$ (a), $\mathbf{k}_T^2 = 10\,\mathrm{GeV}^2$ (b), $\mathbf{k}_T^2 = 20\,\mathrm{GeV}^2$ (c) and $\mathbf{k}_T^2 = 50\,\mathrm{GeV}^2$ (d). The solid, dashed and dash-dotted lines correspond to the KMR, J2003 set 1 and *standard* version of the LDC unintegrated gluon densities, respectively.
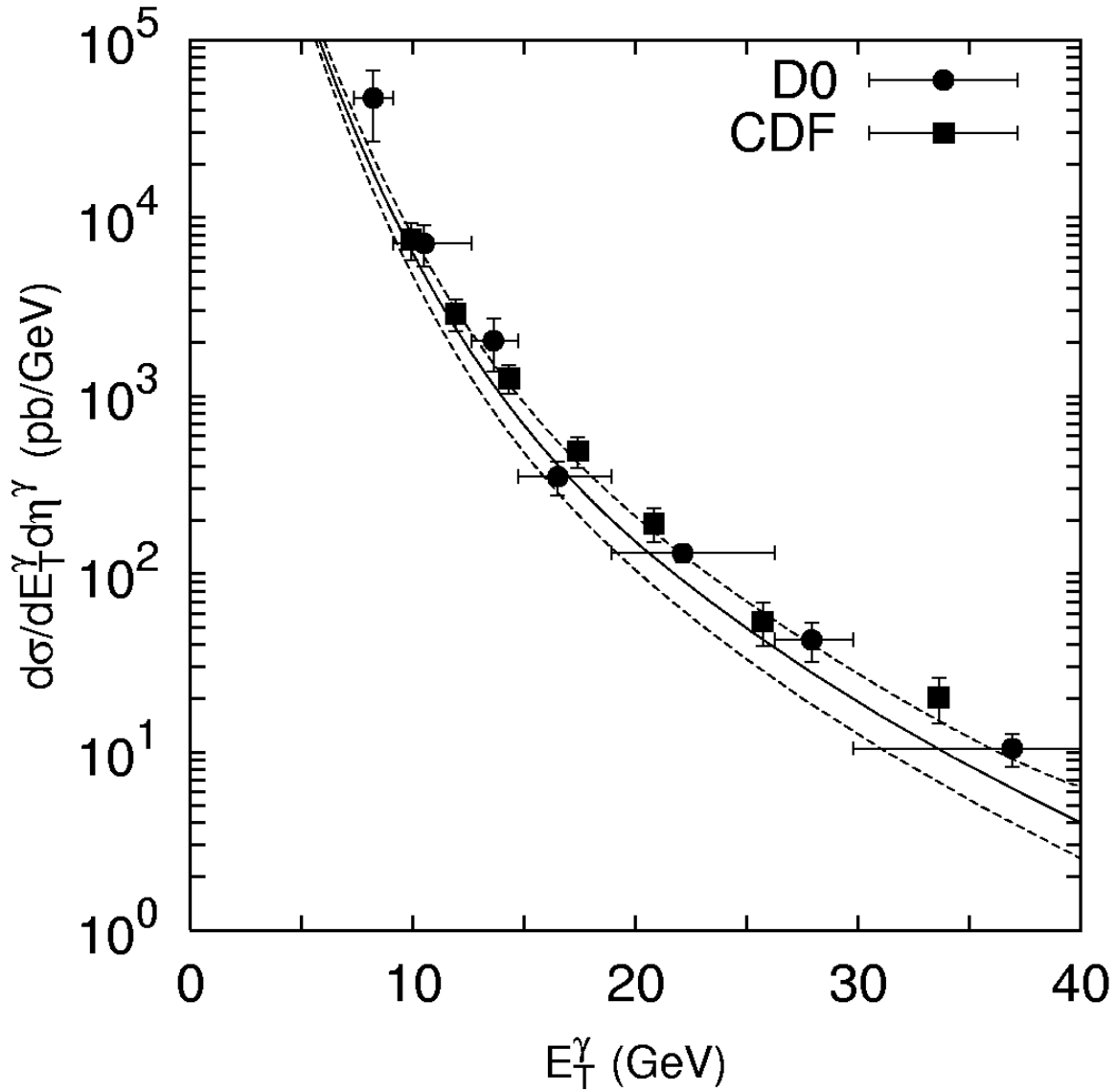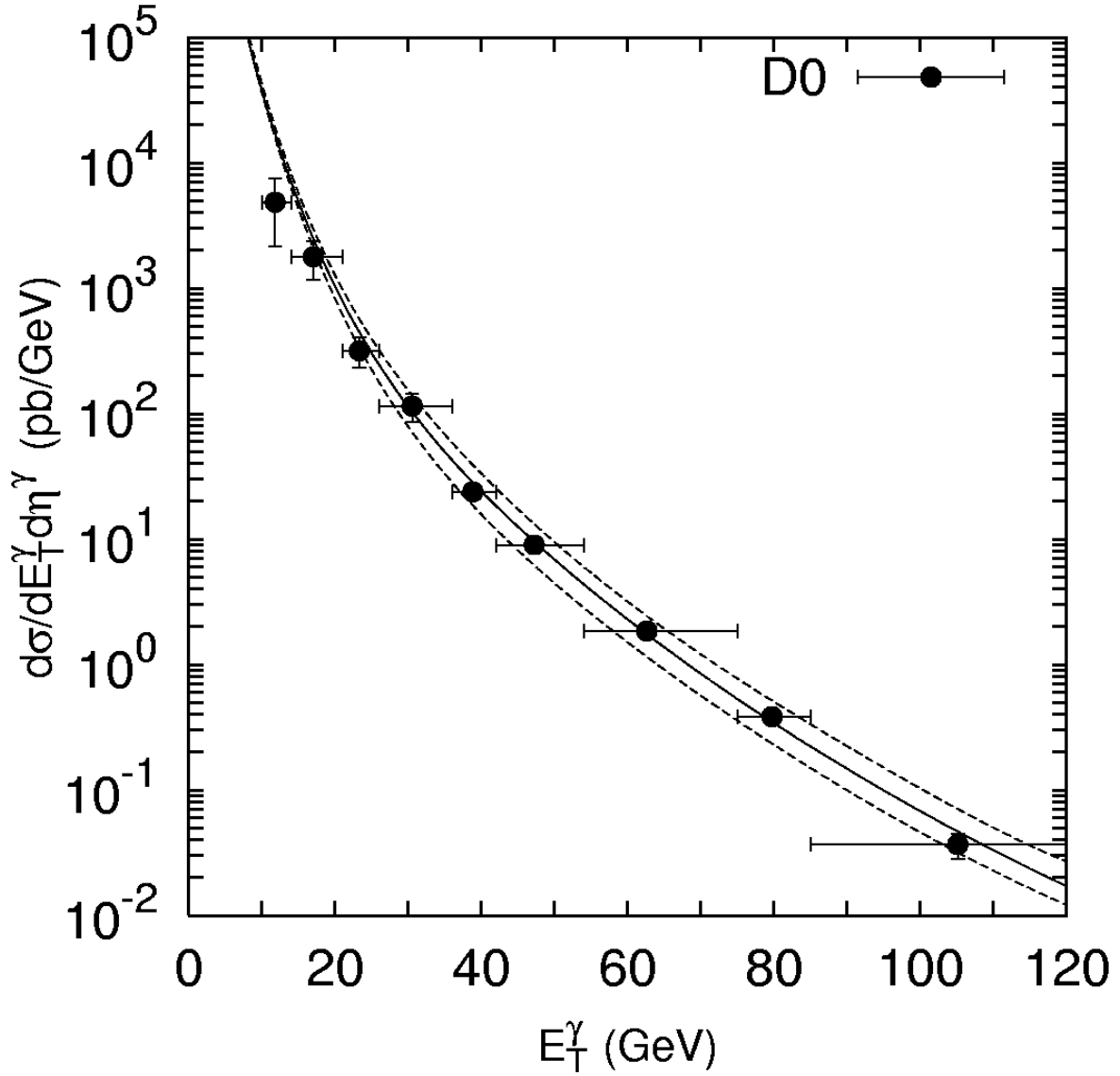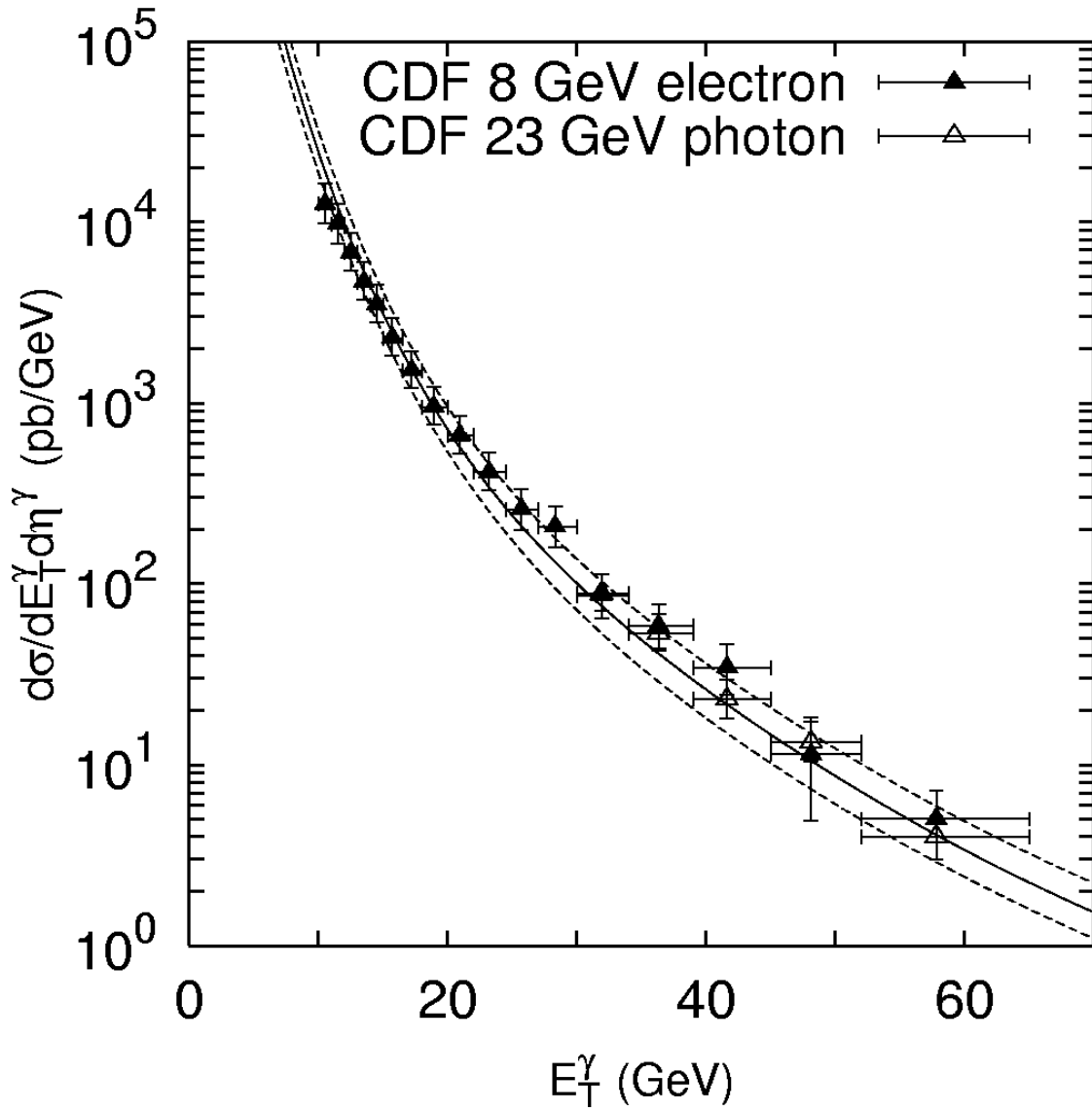
Figure 3: The double differential cross section $d\sigma/dE_T^\gamma d\eta^\gamma$ for inclusive prompt photon hadroproduction at $|\eta^\gamma| < 0.9$ and $\sqrt{s} = 630$ GeV. The solid line corresponds to the default scale $\mu = E_T^\gamma$, whereas upper and lower dashed lines correspond to the $\mu = E_T^\gamma/2$ and $\mu = 2E_T^\gamma$ scales, respectively. The experimental data are from D⊘ [2] and CDF [3].
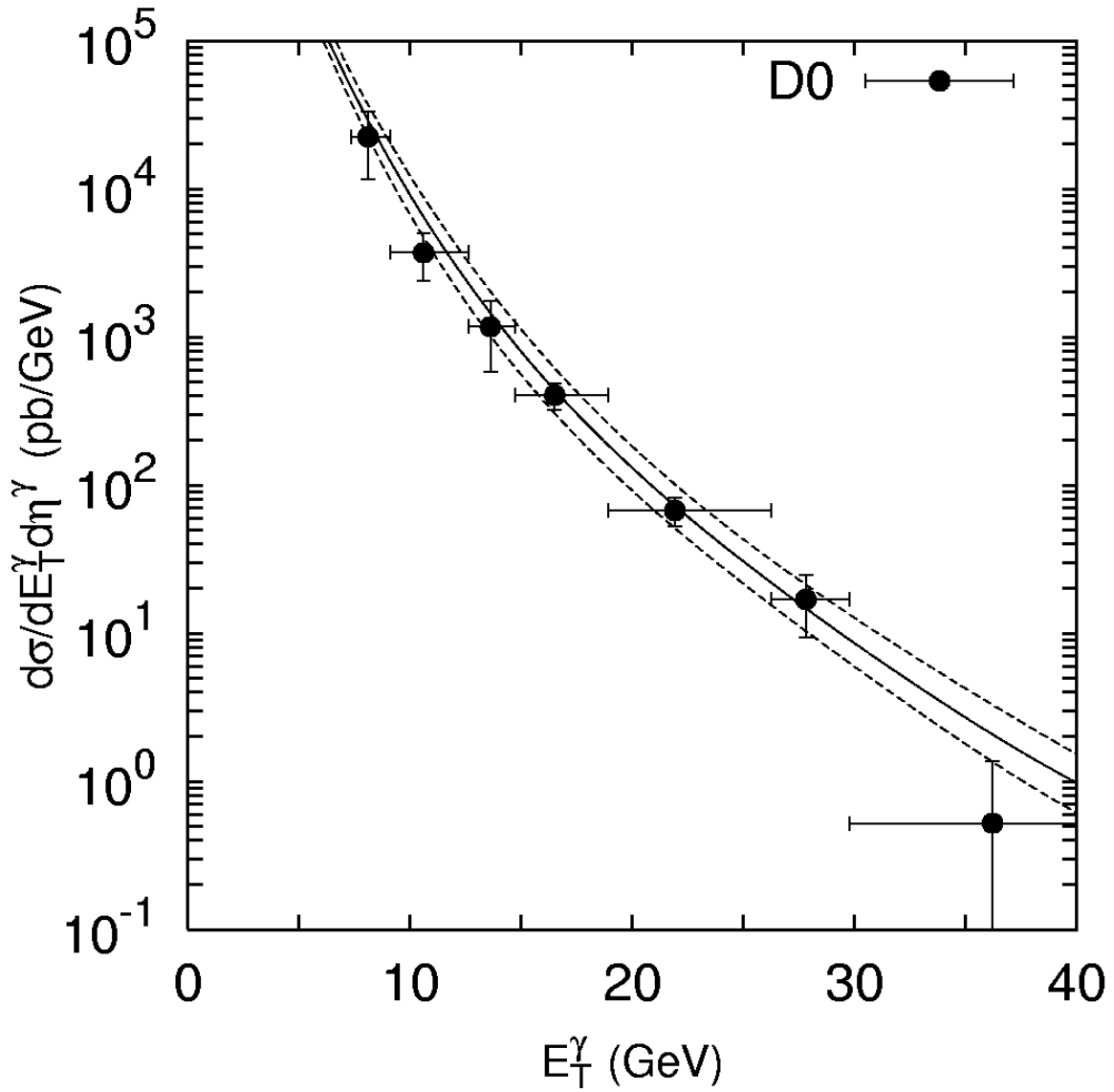
Figure 4: The double differential cross section $d\sigma/dE_T^\gamma d\eta^\gamma$ for inclusive prompt photon hadroproduction at $1.6 < |\eta^\gamma| < 2.5$ and $\sqrt{s} = 630$ GeV. All curves are the same as in Figure 3. The experimental data are from D∅ [2].
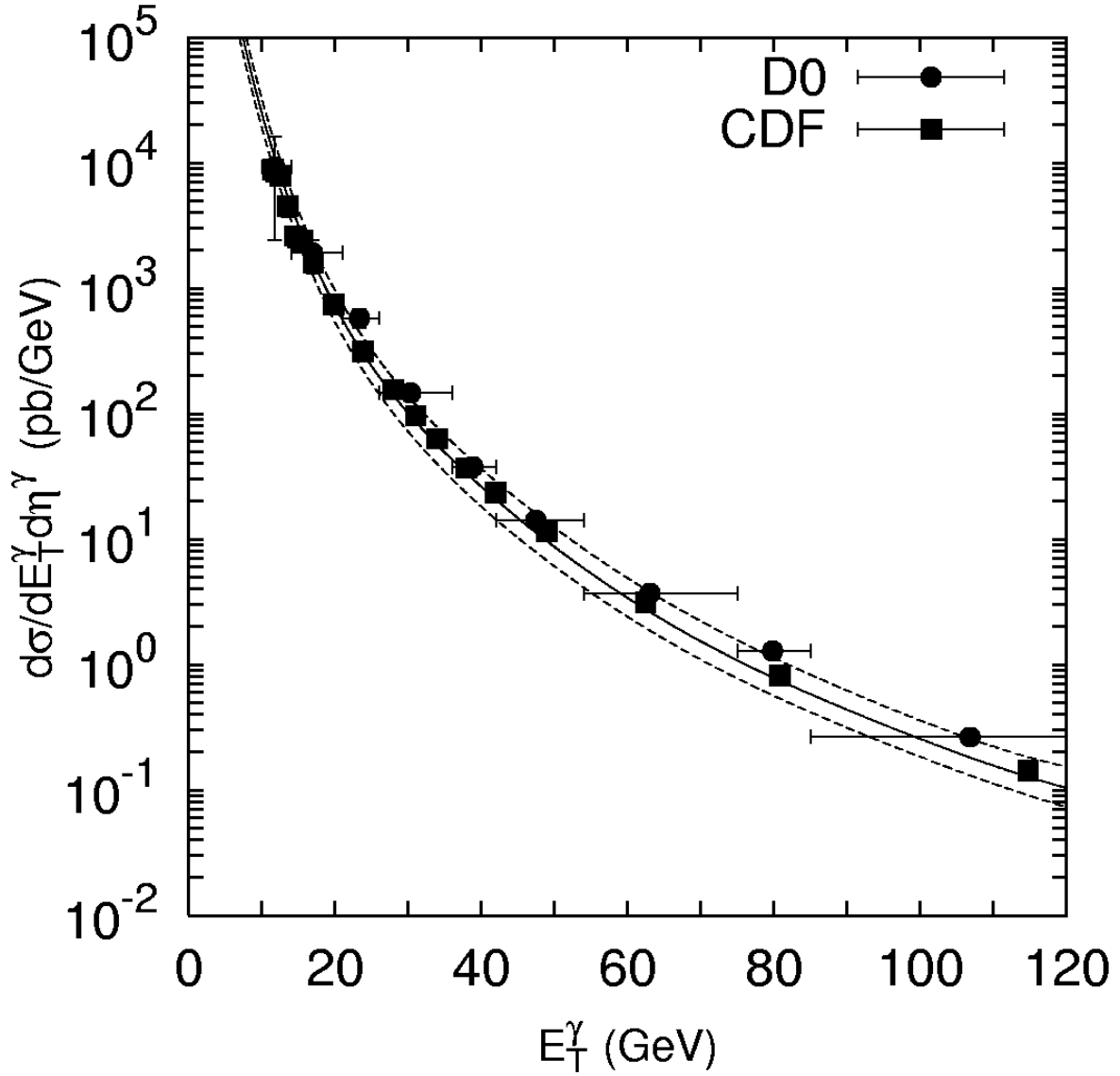
Figure 5: The double differential cross section $d\sigma/dE_T^\gamma d\eta^\gamma$ for inclusive prompt photon hadroproduction at $|\eta^\gamma| < 0.9$ and $\sqrt{s} = 1800$ GeV. All curves are the same as in Figure 3. The experimental data are from D⊘ [1] and CDF [3].

Figure 6: The double differential cross section $d\sigma/dE_T^\gamma d\eta^\gamma$ for inclusive prompt photon hadroproduction at $1.6 < |\eta^\gamma| < 2.5$ and $\sqrt{s} = 1800$ GeV. All curves are the same as in Figure 3. The experimental data are from D$\oslash$ [1].

Figure 7: The double differential cross section $d\sigma/dE_T^\gamma d\eta^\gamma$ for inclusive prompt photon hadroproduction at $|\eta^\gamma| < 0.9$ and $\sqrt{s} = 1800$ GeV. All curves are the same as in Figure 3. The experimental data are from CDF [4].
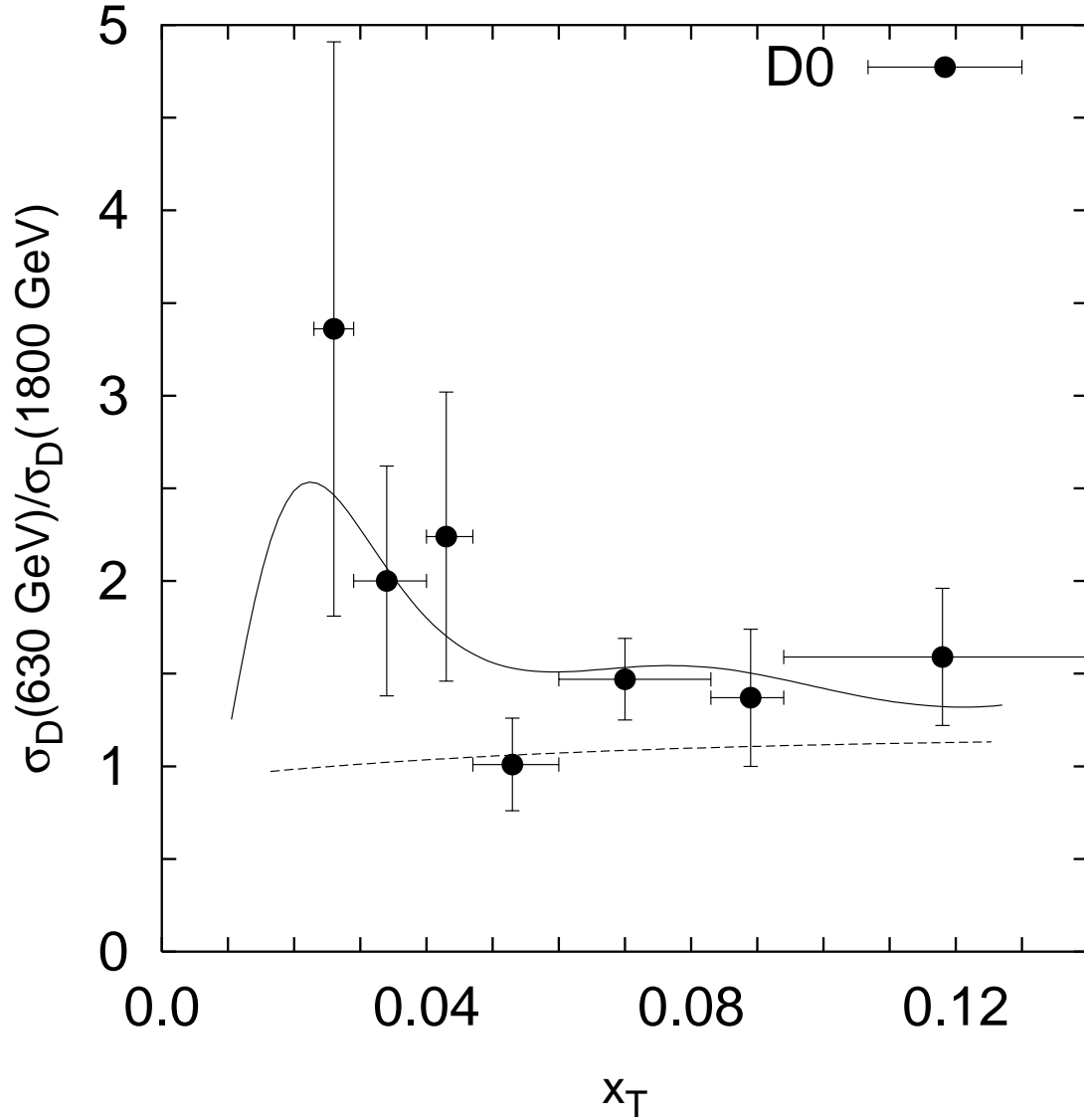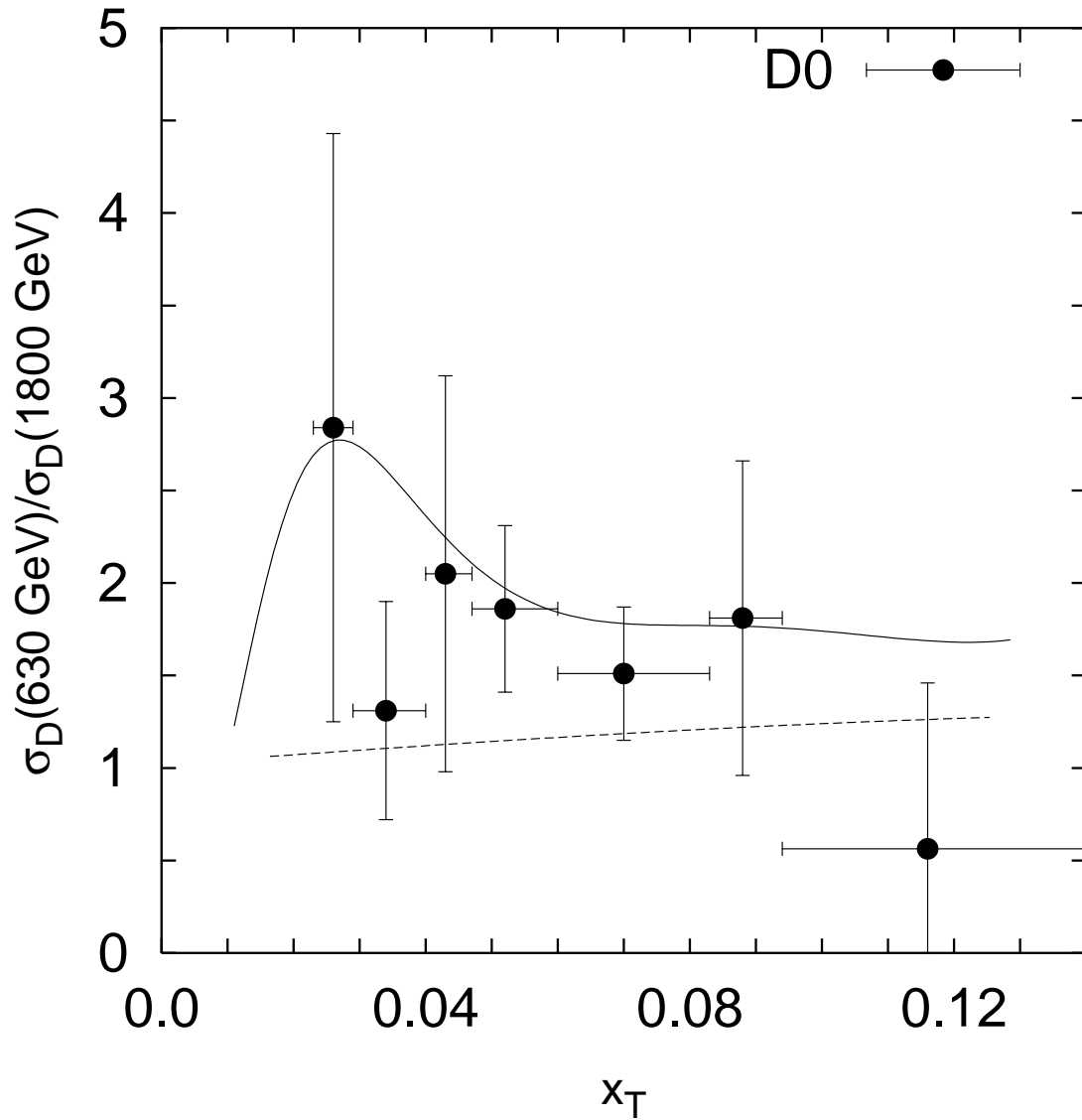
Figure 8: The ratio of the dimensionless cross sections $\sigma_D(630\,\mathrm{GeV})/\sigma_D(1800\,\mathrm{GeV})$ as a function of scaling variable x_T at $|\eta^\gamma| < 0.9$. The solid line was obtained in the k_T-factorization approach whereas dashed line corresponds to the collinear leading-order QCD calculations with the GRV parton densities of the proton. The renormalization and factorization scales are $\mu = E_T^\gamma$. The experimental data are from D$\oslash$ [2].

Figure 9: The ratio of the dimensionless cross sections $\sigma_D(630\,\mathrm{GeV})/\sigma_D(1800\,\mathrm{GeV})$ as a function of scaling variable x_T at $1.6 < |\eta^\gamma| < 2.5$. All curves are the same as in Figure 8. The experimental data are from D∅ [2].
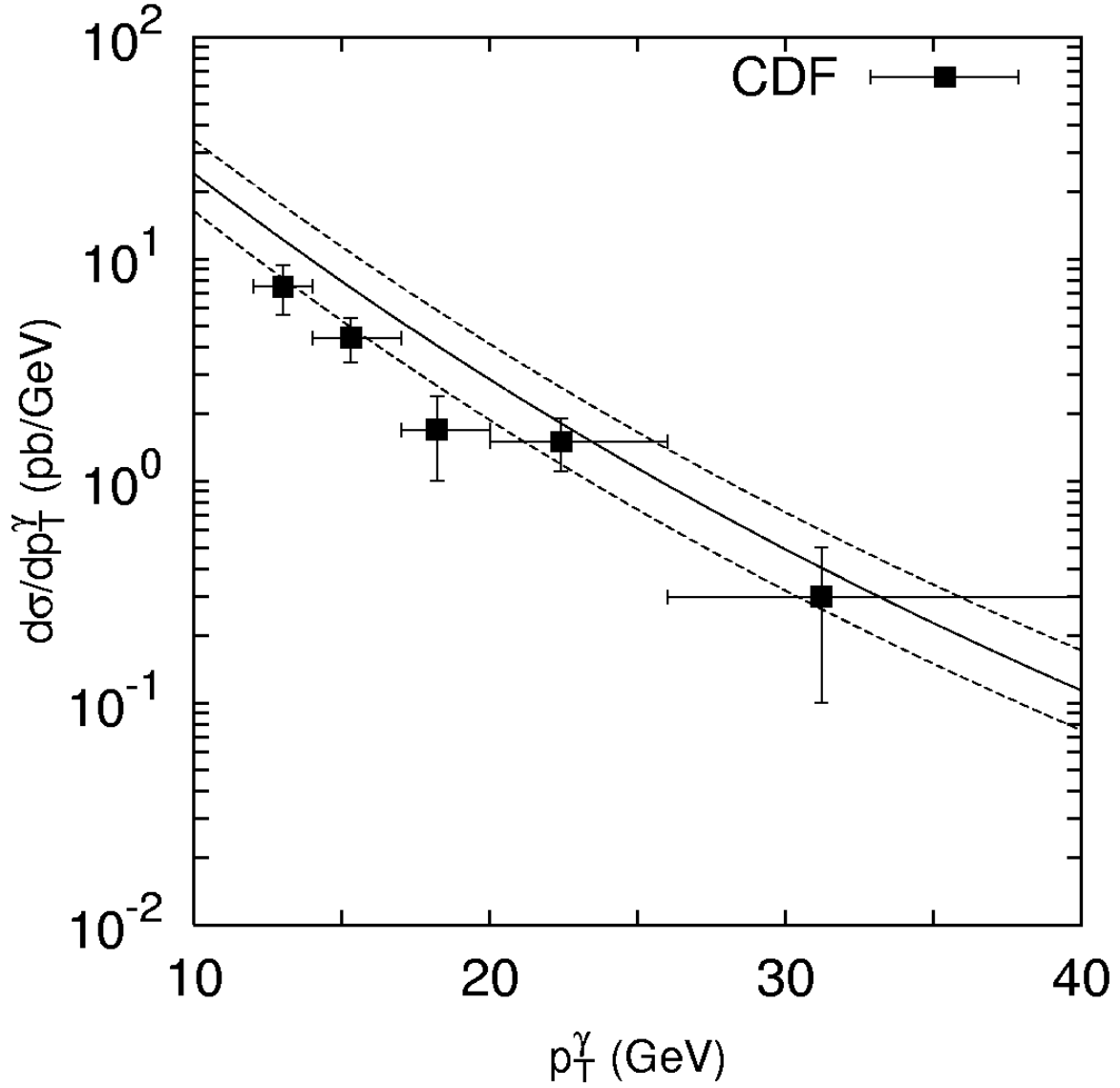
Figure 10: The differential cross section $d\sigma/dp_T^\gamma$ for associated prompt photon and muon hadroproduction at $|\eta^\gamma| < 0.9$, $|\eta^\mu| < 1.0$, $p_T^\mu > 4$ GeV and $\sqrt{s} = 1800$ GeV. All curves are the same as in Figure 3. The experimental data are from CDF [5].
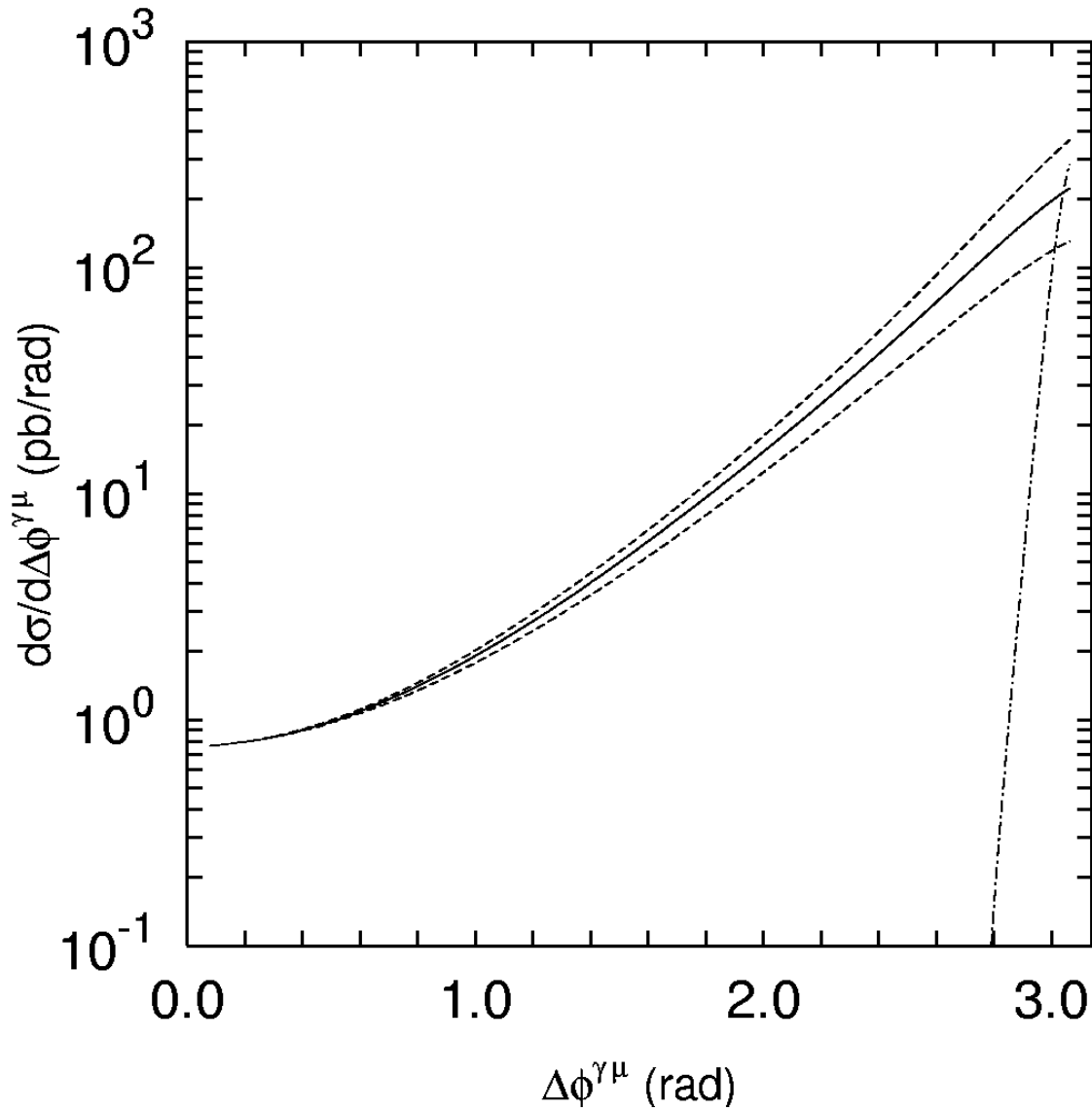
Figure 11: Azimuthal correlations in associated prompt photon and muon hadroproduction at $|\eta^\gamma| < 0.9$, $|\eta^\mu| < 1.0$, $p_T^\mu > 4$ GeV and $\sqrt{s} = 1800$ GeV. The solid line corresponds to the default scale $\mu = E_T^\gamma$, whereas upper and lower dashed lines correspond to the $\mu = E_T^\gamma/2$ and $\mu = 2E_T^\gamma$ scales, respectively. The dash-dotted line correspond to the sole LO QCD calculations at $\mu = E_T^\gamma$.
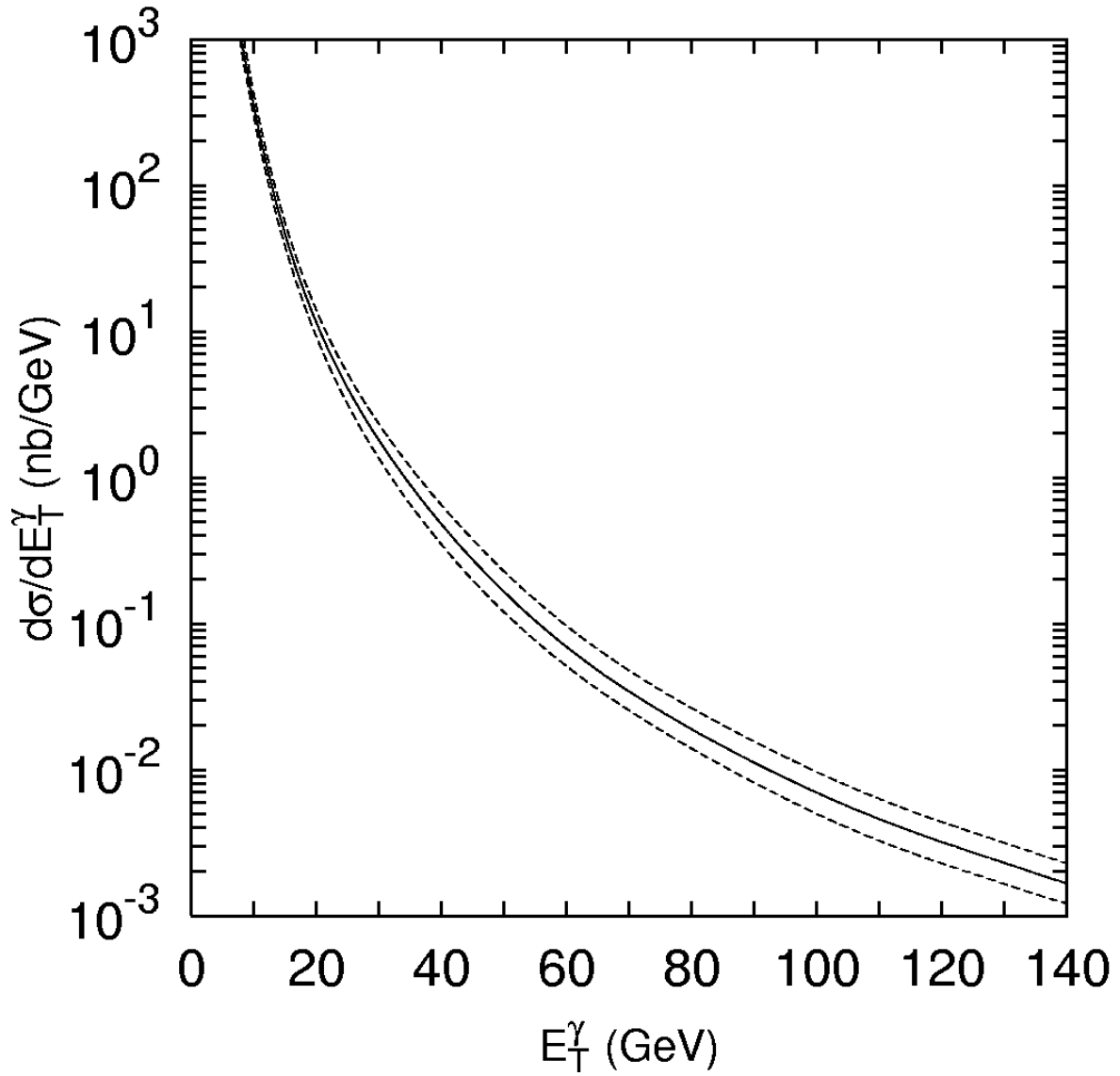
Figure 12: The differential cross section $d\sigma/dE_T^\gamma$ for inclusive prompt photon hadroproduction at $|\eta^\gamma| < 2.5$ and $\sqrt{s} = 14$ TeV. All curves are the same as in Figure 3.
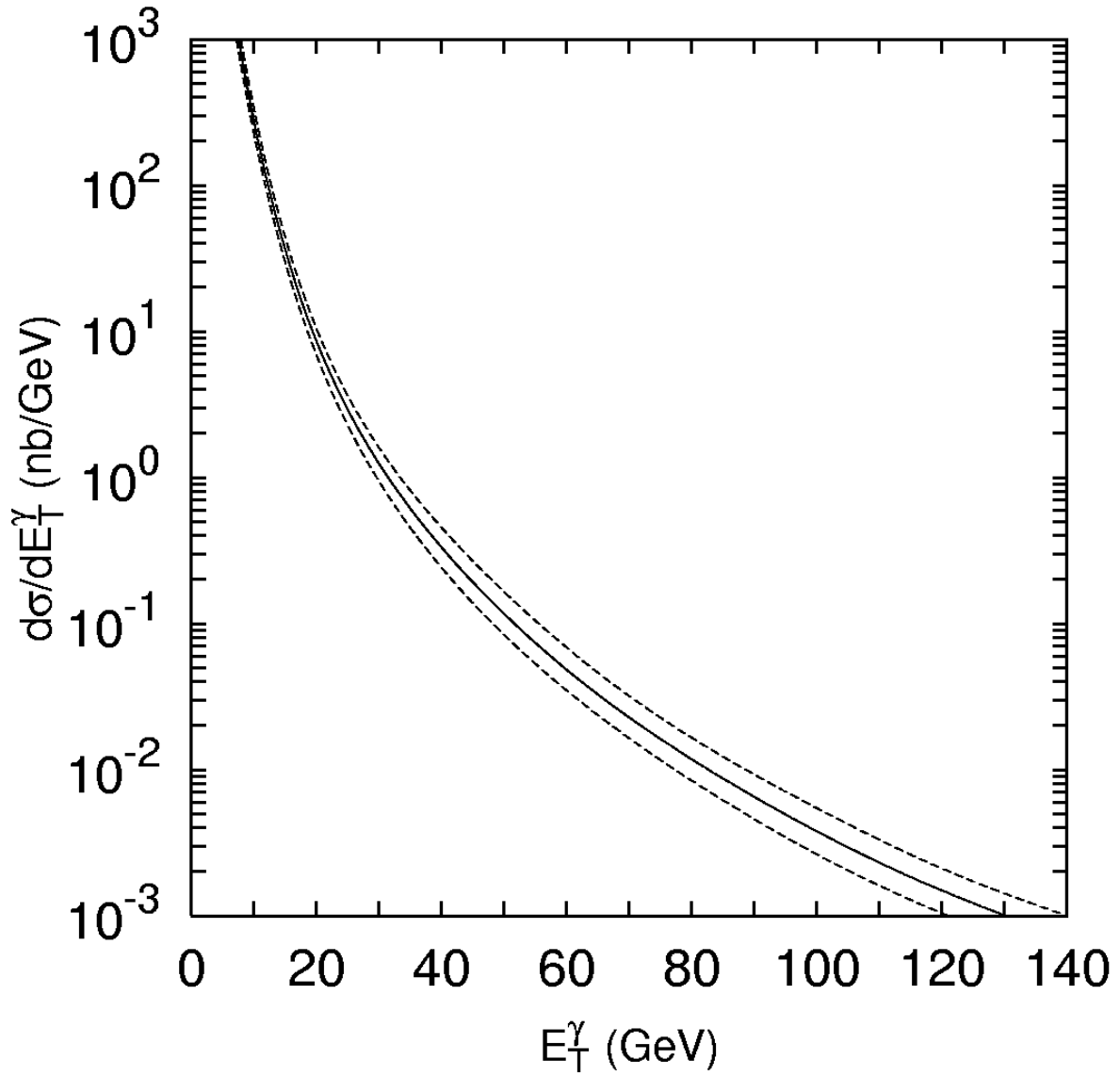
Figure 13: The differential cross section $d\sigma/dE_T^\gamma$ for inclusive prompt photon hadroproduction at $2.5 < |\eta^\gamma| < 4$ and $\sqrt{s} = 14$ TeV. All curves are the same as in Figure 3.